Numerical Characterizations of Viscoplastic Behavior of TA6V with Metallurgical Phase Change

V.Bruyere[1*], C. Touvrey[2], P.Namy[1]
[1]SIMTEC, 8 rue Duployé, 38100 Grenoble, France
[2]CEA DAM, Valduc, 21120 Is-sur-Tille, France
*Corresponding author: vincent.bruyere@simtecsolution.fr

Abstract: In order to predict the residual mechanical state of assemblies during pulsed laser welding, mechanical and metallurgical behaviors of the materials need to be precisely characterized. Based on experimental data and analyses [1], a numerical model is developed in Comsol Multiphysics to take into account the predominant effects (metallurgy influence, viscoplastic behavior) identified for TA6V. To validate our implementation, experimental and numerical results are compared at different temperatures.

Keywords: Welding, Structural Mechanics, Viscoplasticity, Metallurgy.

1. Introduction

Spot laser welding is generally used in industrial applications due to its main advantage: it generates very located temperature gradients and therefore, induces small distortions in the pieces. Nevertheless, the prediction of residual stresses or strains can be useful to precisely design assemblies. Different steps are required to achieve this goal. In a previous study [2], a thermo-hydraulic model has been built to obtain the shapes of Fusion Zone (FZ) and Heat Affected Zone (HAZ), from operating conditions and material properties. Based on this knowledge, an equivalent heat source can be determined to model the laser power and the thermo-mechanical problem can be solved. However, in order to obtain precise results, the thermo-mechanical behavior of TA6V and its metallurgical characteristics must be considered. Based on experimental data and analyses, a characterization model is built with Comsol Multiphysics and presented here.

2. Physical Phenomena and Modeling

Spot laser welding leads to strong temperature variations. For example, in industrial operating conditions, the boiling point of the TA6V can be reached in less than one millisecond. Depending on the intensity of the thermal loading and its kinetics, the resulting micro-structure of TA6V after cooling can then be strongly affected. Metallurgical phase changes occur and strongly affect the mechanical properties. Moreover, the mechanical behavior at high temperature becomes highly non-linear and viscoplastic effects have to be taken into account.

2.1 Metallurgical states

As detailed in the literature [1][3], three different metallurgical phases are classically encountered in TA6V, depending on temperature and heating or cooling kinetics.
At ambient temperature, it is assumed to be composed of 92% of α-phase and 8% of β-phase. When the temperature becomes higher than the martensitic temperature, T_m ($\approx 800°C$), but remains lower than T_β ($\approx 1000°C$), a metallurgical phase change occurs. The volume fraction of β-phase highly increases, depending on heating kinetics. For higher temperatures (under the melting point), the material is only composed of β-phase. During the cooling process, this β-phase is partially or totally transformed in α'-phase, and the three phases can coexist. The time-evolution of these three-phase volume fractions can be expressed by Ordinary Differential Equations (ODE's) as a function of temperature, T, and its variation with time, $\dot{T}$, as follows:

α-phase:

$$\dot{z_\alpha} = \begin{cases} z_\alpha * \dfrac{z^c_{max}(T) - z_\alpha - z_{\alpha'}}{\tau_\alpha(T)} & if\ (T < T_\beta) \\ z_\alpha * \dfrac{z^h_{max}(T) - z_\alpha - z_{\alpha'}}{\tau_\alpha(T)} & if\ (T > T_\beta) \end{cases}$$

α'-phase:

$$\dot{z_{\alpha'}} = \begin{cases} z_{\alpha'} * \dfrac{z^c_{max}(T) - z_\alpha - z_{\alpha'}}{\tau_{\alpha'}(T)} & if\ (\dot{T} > 0) \\ -\dfrac{z_\beta}{\tau_B(T)}\dot{T} & if\ (\dot{T} < 0) \end{cases}$$

β-phase:

$$z_\beta = 1 - z_\alpha - z_{\alpha'}$$

with z_i the volume fraction of phase i, $z^c_{max}(T)$, $z^h_{max}(T)$, $\tau_\alpha(T)$, $\tau_{\alpha'}(T)$ and $\tau_B(T)$, functions of temperature obtained from experimental data [1].

2.2 Thermo-mechanical behavior

At high temperatures, the behavior of TA6V is highly non-linear and viscoplastic effects have to be taken into account to estimate stress and strain states.
First of all, the strain tensor ($\underline{\underline{\varepsilon}}$) is classically shared in two parts: the elastic strain tensor ($\underline{\underline{\varepsilon}}^e$) and the plastic tensor ($\underline{\underline{\varepsilon}}^p$):

$$\underline{\underline{\varepsilon}} = \underline{\underline{\varepsilon}}^e + \underline{\underline{\varepsilon}}^p$$

Secondly, the constitutive relation between the stress tensor ($\underline{\underline{\sigma}}$) and the strain tensors, is expressed as follows, taking into account the thermal expansion:

$$\underline{\underline{\sigma}} = \underline{\underline{\underline{\underline{\mathbb{E}}}}}(T) : \left(\underline{\underline{\varepsilon}} - \underline{\underline{\varepsilon}}^p - \alpha(T, z_i) \cdot (T - T_0)\underline{\underline{\boldsymbol{I}}}\right)$$

with $\underline{\underline{\underline{\underline{\mathbb{E}}}}}(T)$, the 4th-order elasticity tensor function of $E(T)$, the Young modulus and $\nu(T)$ the Poisson coefficient; $\alpha(T, z_i)$, the coefficient of thermal expansion and T_0 a reference temperature.

As proposed in [1], the "Lemaitre and Chaboche" model [4] can be used to describe viscoplastic flow and non-linear hardening of TA6V. A similar approach has been previously developed in Comsol Multiphysics by Roger et al. [5] for another material. In this work, and based on experimental results [1], the isotropic hardening can be neglected. On the other hand, non-linear kinematic hardening has to be considered. A "back stress" tensor, $\underline{\underline{X}}$, is defined, linked to the plastic strain rate tensor $\underline{\underline{\dot{\varepsilon}}}^p$ and the effective strain rate $\dot{p}$. The complete system of equations which describes this viscoplastic flow with non-linear kinematic hardening is expressed by:

$$\underline{\underline{\dot{\varepsilon}}}^p = \dot{p}\frac{3}{2}\frac{\underline{\underline{\sigma}}' - \underline{\underline{X}}'}{J_2\left(\underline{\underline{\sigma}}' - \underline{\underline{X}}'\right)}$$

$$\underline{\underline{\dot{X}}} = \frac{2}{3}C(T)\underline{\underline{\dot{\varepsilon}}}^p - \gamma\underline{\underline{X}}\,\dot{p}$$

$$\dot{p} = \left\langle \frac{J_2\left(\underline{\underline{\sigma}} - \underline{\underline{X}}\right) - \sigma_y(T)}{K(T)} \right\rangle^{\mathrm{n(T)}}$$

with $\sigma_y(T)$, the yield stress, $C(T)$ and γ, two kinematic hardening coefficients and $K(T, z_i)$ and $n(T, z_i)$, two coefficients of viscoplasticity.

The notation $\underline{\underline{A'}}$ represents the deviatoric part of a tensor $\underline{\underline{A}}$. The bracket notation $\langle A \rangle$ is the positive part of A and the J_2 notation is the second deviator invariant of the considered tensor.
At last, the quasi-static equation of motion is solved for by using the "Solid Mechanics" physics:

$$\nabla \cdot \sigma = 0$$

3. Numerical implementation

3.1 Metallurgy

A first 0D-model is built to obtain the three-phase metallurgical evolution as a function of time. Two "Point ODEs" are then defined and solved in a coupled way. The third volume fraction is the complement of the others.
An analytical expression of the temperature evolution as a function of time is set with constant heating and cooling kinetics, as shown Figure 1:

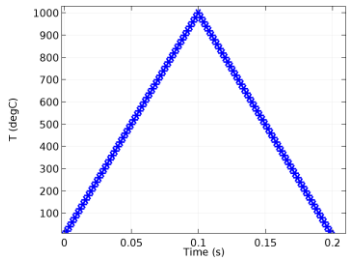

Figure 1. Temperature evolution with $\dot{T} = \pm 10000°C/s$

3.2 Tensile Testing

Tensile tests are numerically performed to validate the model chosen to describe the thermo-mechanical behavior of the material.
The geometry of the tensile specimen used in experiments is shown on the left, Figure 2. A 2D-axisymmetric model is built by using symmetries of the geometry.

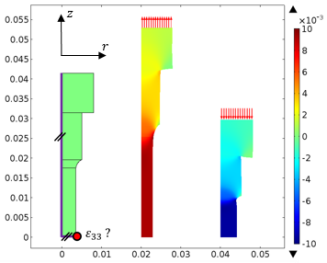

Figure 2. Geometry of the tensile specimen at initial state on the left, during tension on the middle and during compression on the right, colored by local strain tensor component, ε_{33}

Concerning boundary conditions, the velocity is prescribed in the z-direction on the top of the specimen:

$$\frac{\partial w}{\partial t} = \dot{\varepsilon}_{st} L_0 \cdot f(t)$$

with $\dot{\varepsilon}_{st}$ a constant strain rate, L_0 a reference length and $f(t)$ a time-function, which worth 1 for a tensile loading and -1 for a compression one.

To compare with experimental data, 4 load/unload cycles are performed and the local strain component, $|\varepsilon_{33}|$, is constraint to be lower than 0.01.

4. Results

4.1 Metallurgical phases

The evolution of each metallurgical phase is plotted on the right, Figure 3, and compared with results from the literature [1] (on the left, Figure 3) for a temperature kinetics of $10000°C/s$.

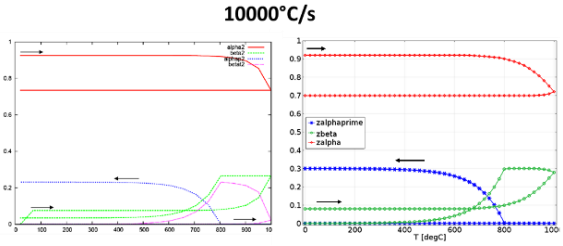

Figure 3. Volume fractions of each metallurgical phase from [1] (on the left) and our COMSOL approach (on the right)

At ambient temperature ($T = 20°C$), the material is composed of 92% of α-phase (in red, Figure 3), 0% of α'-phase (in blue, Figure 3) and 8% of β-phase (in green, Figure 3). The material is firstly heated as shown Figure 1 (arrows to the right, Figure 3). The volume fraction of each phase remains constant while the temperature is lower than the T_m temperature. When $T_m \leq T \leq T_\beta$, the fraction of α-phase decreases and β-phase fraction increases. At $T = T_m$, the cooling stage starts, the fraction of α-phase remains constant and when $T \leq T_m$, the α'-phase appears from the β-phase. This simple model can be used to obtain the repartition of each phase as a function of the temperature and its variation with time. Concerning the comparison between both approaches, a satisfying agreement is obtained.

4.2 Viscoplastic behavior

In order to describe the viscoplastic behavior of the material, the evolution of different stresses is plotted in Figure 5 for one cycle and at one point (in red Figure 2), as a function of local strain (Figure 5, top) and as a function of time (Figure 5, bottom):

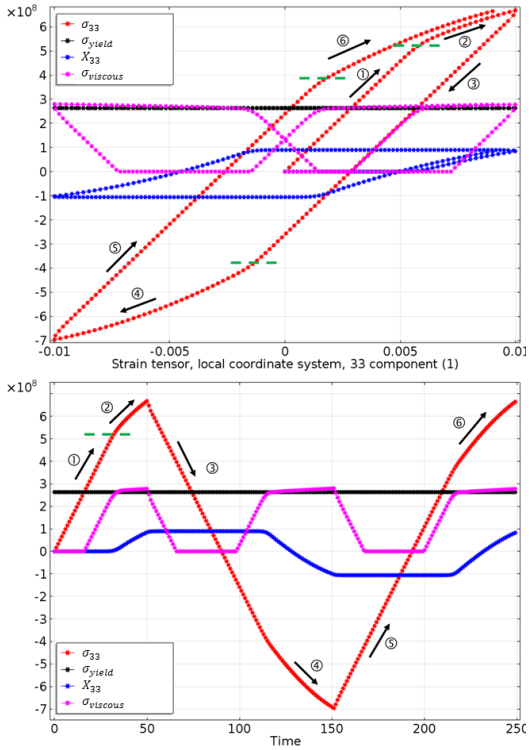

Figure 4. Stresses evolution for a load/unload cycle

①: At initial state, the strain/stress tensors are zero. The velocity is numerically set at the top of the specimen and the tensile test starts. First of all, the normal stress, σ_{33}, linearly increases (in red, Figure 4). Then, it exceeds the yield strength (in black, Figure 4) and because of viscous effects, plasticity only begins when the viscous stress, $\sigma_{viscous} = K\dot{p}^{\frac{1}{n}}$ (in magenta, Figure 4), reaches this point.

②: The relation between stress and strain is not linear anymore and the kinematic hardening starts. The "backstress" X_{33} increases (in blue, Figure 4).

③: When the predefined maximum of strain ($\varepsilon_{33} = 0.01$) is reached, the velocity becomes negative and the unloading begins. The normal stress linearly

decreases and the back stress remains constant. Indeed, kinematic hardening is considered here. The unload strength must be lower than the load strength, due to the "Baushinger effect". This is taken into account in the model by the "back stress" which "shifts" the starting point of the plasticity.

④: The viscoplastic flow starts thus "earlier" in compression, when the viscous stress reaches the yield stress. The viscoplastic flow lasts longer and the limit strain $\varepsilon_{33} = -0.01$ is finally reached.

⑤: The velocity orientation changes again and normal stress linearly increases. The back stress remains constant until the viscous stress exceeds the yield point.

⑥: Plasticity starts for a lower stress value than for the first loading ($\approx 120Pa$ lower) and because isotropic hardening is not considered for this material, the load surface remains quasi-constant for the other cycles.

4.3 Temperature influence

In order to calibrate our model, experimental data and analyses from [1] are used here. Four temperature values are firstly studied for a constant strain rate value of $\dot{\varepsilon}_{st} = 10^{-3}s^{-1}$. The resulting strain/stress evolutions are shown in Figure 5 for a case where $z_\alpha = 1$.

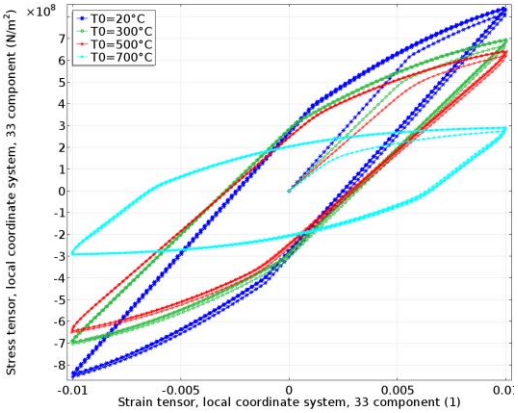

Figure 5. Temperature influence on stress/strain evolution

As expected, the higher the temperature, the lower the Young modulus and the yield point. The hardening also decreases with temperature.

Comparison between numerical and experimental results is illustrated Figure 6 for eight temperatures and a constant strain rate of $10^{-3}s^{-1}$.

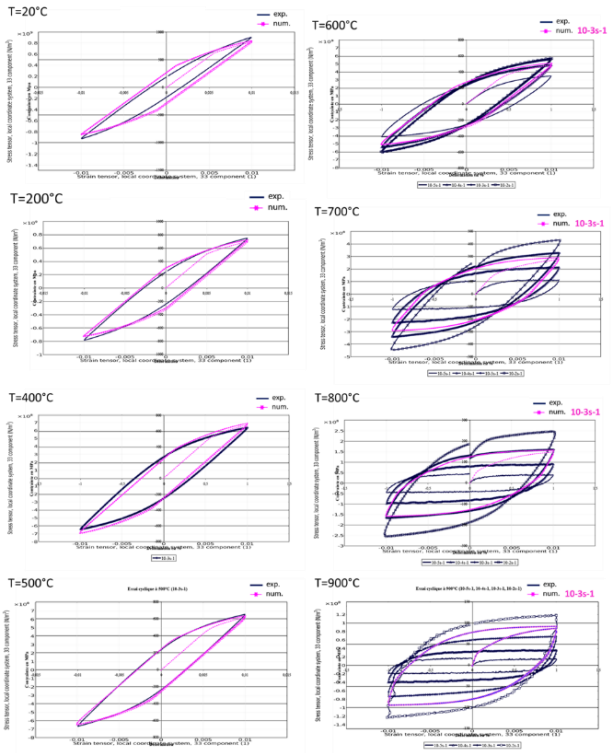

Figure 6. Comparison between experimental results from [1] (blue) and our numerical results (magenta)

Numerical results are in satisfying agreement with the experimental ones for each temperature. The implementation of the model as well as the coefficient values used for this material can thus be validated.

4.4 Strain rate influence

To complete this study, the influence of the strain rate, $\dot{\varepsilon}_{st}$, used to define the velocity of the specimen, is considered here. Indeed, as seen previously, at high temperature, TA6V becomes more ductile and viscous effects, linked to time variations, have to be taken into account.

Height tests are performed at four different strain rates ($10^{-2}s^{-1}$ in blue, $10^{-3}s^{-1}$ in green, $10^{-4}s^{-1}$ in red and $10^{-5}s^{-1}$ in cyan, Figure 7) and two temperatures $T = 200°C$ and $T = 700°C$.

Numerical results are plotted on the right of Figure 7 and compared with experimental results on the left of Figure 7.

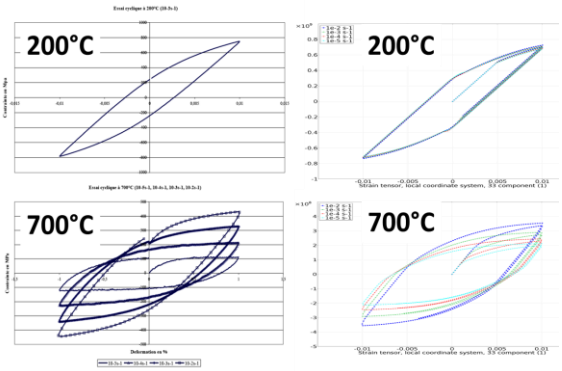

Figure 7. Comparison between experimental results from [1] (on the left) and our numerical results (on the right)

At low temperature ($200°C$), viscous effects are negligible and strain rate has no influence on the stress/strain state. Indeed, the n-exponent in the viscosity law is higher for lower temperature. When temperature increases ($700°C$), this coefficient decreases and the material behavior becomes time-dependent. Viscoplastic effects are preponderant and must be taken into account to estimate the residual stresses for example.
For low strain rate values, some differences are observed between numerical and experimental values. It can be explained by the kinematic hardening "restoration process" [4], that is not taken into account in this work. Nonetheless, same tendencies are qualitatively found numerically and experimentally concerning the global stress/strain evolution.

5. Conclusions

A metallo-thermomechanical model has been developed to describe the behavior of TA6V under thermal loading. Based on experimental data, satisfying agreements have been found for each comparison, validating the numerical implementation. The model can now be applied for industrial operating conditions to estimate the residual stress and strain states of assemblies.

6. References

1. Y. Robert, Simulation numérique du soudage du TA6V par laser YAG impulsionnel : caractérisation expérimentale et modélisation des aspects thermomécanique associées à ce procédé, *Phd Thesis* (2007)
2. V. Bruyere et al., A Phase Field Approach to Model Laser Power Control in Spot Laser Welding, *Proceedings of the 2014 Comsol Conference Cambridge* (2014)
3. Y. Combres et al., Traitements thermiques des alliages de titane, *Techniques de l'ingénieur* (1995)
4. J. Lemaitre et al., *Mécanique des matériaux solides*, 3rd edition, Dunod (2009)
5. F. Roger et al., Modeling Residual Stresses in Arc Welding, *Proceedings of the 2010 Comsol Conference Boston* (2010)